Graphical Abstract (for review)

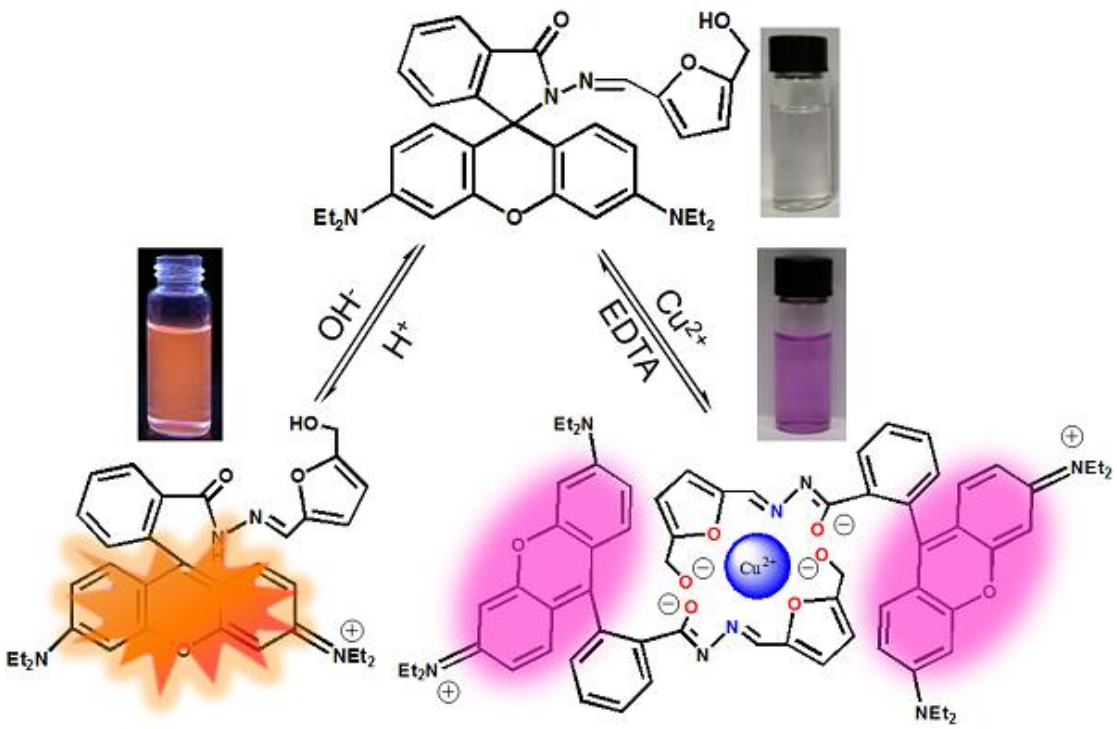

5-Hydroxymethylfurfural modified rhodamine B dual-function derivative: Highly sensitive and selective optical detection of pH and Cu^{2+}

Enze Wang [a], Yanmei Zhou [a,*], Qi Huang [a], Lanfang Pang [a], Han Qiao [a], Fang Yu [a], Bin Gao [b], Junli Zhang [c], Yinghao Min [a], Tongsen Ma [a]

[a] *Institute of Environmental and Analytical Sciences, College of Chemistry and Chemical Engineering, Henan University, Kaifeng, Henan 475004, P.R. China*

[b] *Department of Agricultural and Biological Engineering, University of Florida, Gainesville, FL 32611*

[c] *Key Laboratory of Plant Stress Biology, Henan University, Kaifeng 475004, PR China*

* Correspond author: Tel: +86-371-22868833-3422; Fax: +86-371-23881589
E-mail address: zhouyanmei@henu.edu.cn (Y.M. Zhou)

Abstract: A dual-function optical chemosensor (RBF) was designed and easily synthesized by condensation reaction of 5-Hydroxymethylfurfural and rhodamine B hydrazide. RBF exhibited highly sensitive, highly selective and quick response to acidic pH. The fluorescence intensity of RBF exhibited a more than 41-fold increase within the pH range from 7.50 to 3.73 with a pKa value of 5.02, which could be successfully applied to monitor intracellular pH in living PC12 cells and Hela cells. Additionally, the spectroscopy of UV-Vis and EDTA-adding experiments indicated that RBF was a highly selective and reversible colorimetric chemosensor for Cu^{2+} in Tris-HCl (10 mM, pH=7.2) aqueous buffer solution as well as other metal ions had no obvious interference. Moreover, RBF has been successfully applied to detect Cu^{2+} in real water samples.

Keywords: Rhodamine B, Fluorescent, pH, Cu^{2+}, Colorimetric, Live-cells imaging

1. Introduction

pH plays a fundamental role in various systems [1-4], especially within cells [5] such as apoptosis [6,7] and cell growth [8,9], signal transduction [10] and autophagy [11,12]. Abnormal intracellular pH values indicate abnormal cell events and are observed in some diseases including cancer and Alzheimer's disease[19]. Many methods for measurement of pH values have achieved highly successful including nuclear magnetic resonance [13], microelectrodes [14], acid-base indicator titration [15], potentiometric titration [16] and fluorescent probes. On the other hand, among the heavy- and transition-metal (HTM) ions, Cu^{2+} plays a very crucial role in several physiological processes in organisms [17]. Especially, it is a cofactor for plentiful enzymes. The total Cu^{2+} content of the adult human body usually contain 70-80 mg under normal conditions [18]. It exhibits toxicity to certain biological systems under overload conditions, however, Cu^{2+} in abnormal levels is connected to oxidative stress and neurological disorders such as Parkinson's, Alzheimer's, Menkes', and Wilson's diseases [19-22]. Similarly, there are many methods for measurement of Cu^{2+}. Optical chemosensors have been made more attractive among these methods owing to their operational simplicity, high sensitivity, low-cost and real-time detection [23, 24].

As an excellent model, rhodamine B framework relies on its long absorption and emission wavelength, large absorption coefficient and high fluorescence quantum yield [25]. Rhodamine B derivatives with a spirocyclic structure are colorless and non-fluorescent, while the ring-opening of spirocyclic structure exhibits a pink color and a strong fluorescence emission. This makes rhodamine B derivatives serve as

excellent “off-on” fluorescent probes. To date, a great number of optical chemosensors based on rhodamine B have been widely developed as “off-on” fluorescent or colorimetric chemosensors for the detection of metal ions, such as Hg^{2+} [26-30], Al^{3+} [31-34], Fe^{3+} [35-37], Pb^{2+} [38], Cr^{3+} [39,40], Cu^{2+} [41-46] and Pd^{2+} [47]. There are also many fluorescent chemosensors for the measurement of intracellular pH [48-54]. To the best of our knowledge, a hugely limiting factor of the above rhodamine B probes is that they can detect only the same kind of analytes using fluorescence and UV-Vis absorption spectrometry method at the same time. Furthermore, although dual-function fluorescent chemosensors designed for detecting different metal ions are plentiful [55-59], for pH and metal ions using different optical signals are relatively few [60].

As a continuation of our research efforts devoted to fluorescent probes for metal ions recognition, we designed and synthesized a bifunctional rhodamine B chemosensor (RBF) exhibited not only highly sensitive for pH but also highly selective recognition of Cu^{2+} by fluorescent and colorimetric detection, respectively. The chemosensor (RBF) with a pKa value of 5.02 showed great enhanced fluorescence intensity and visible color changes from colorless to pink over a pH range from 7.50 to 3.73, which was suitable for monitoring intracellular pH in living cells. Furthermore, the feasibility of the chemosensor (RBF) for detecting Cu^{2+} in real water samples was also investigated.

2. Experimental

2.1. Apparatus

^{1}H and ^{13}C NMR spectra were measured on a Bruker DMX-300 spectrometer operating at 400 MHz. The MS spectra were performed on Bruker ESQUIRE HPLC-MS AB 4000Q. UV-Vis absorption spectra were recorded on a U-4100 spectrophotometer. Fluorescent spectra were recorded on a Hitachi F-7000 FL spectrofluorometer. FT-IR spectra were measured on Thermo Nicolet AVATAR360 spectrometer. An Olympus Zeiss 710 laser scanning confocal microscopy was used for fluorescence image of cells. The pH measurements were measured by use of a PHS-3D digital pH-meter (Jingke, Shanghai). All measurements of spectra were carried out in aqueous solution with 1% ethanol as cosolvent.

2.2. Materials

Rhodamine B was purchased from Beijing chemical plant, 5-Hydroxymethylfurfural was purchased from J&K, Hydrazine hydrate was purchased from Tianjin reagent plant. The solution of metal ions was prepared from their nitrate salts and chloride salts of analytical grade. The solvents were used as received without further purification. Distilled water was used throughout. Britton-Robinson (B-R) buffer was prepared with 40 mM acetic acid, boric acid, and phosphoric acid. Dilute hydrochloric acid or sodium hydroxide was used for adjusting pH values. Tris-HCl aqueous buffer solutions (10 mM, pH=7.20) were prepared using 20 mM Tris(hydroxymethyl)aminomethane (Tris) and proper amount of HCl under adjustment by pH meter.

2.3. Cells culture

PC12 cells were seeded in glass bottom culture dishes and grown in Dulbecco's

113 modified Eagle's medium (DMEM) supplemented with 2.5% fetal bovine serum (FBS)
114 and 15% horse serum at 37°C with 5% CO_2 atmosphere. HeLa cells were cultured in
115 DMEM supplemented with 10% FBS, 100 μg/ml penicillin and 100 μg/mL
116 streptomycin in the same incubator environment until harvesting for the experiment.
117 When harvesting, the DMEM was drawn out from the culture dishes, and the dishes
118 were rinsed three times with 10 mM phosphate buffer saline (PBS) and then treated
119 with 4 mL trypsinase solution containing 0.25% EDTA for 3 min in the incubator. The
120 cells were centrifuged at 1500 rpm for 5 min, then removed the supernatant.

121 2.4. Synthesis of RBF

122 RBF was facilely synthesized by simple condensation reaction of Rhodamine B
123 Hydrazide (RBH) and 5-Hydroxymethylfurfural. The synthesis and structure of RBF
124 were depicted in Scheme 1. RBH was synthesized according to the literature methods
125 by a one-step reaction of rhodamine B with hydrazine hydrate (80%) in ethanol [61].
126 To a 100 mL round-bottomed flask, RBH (2.19 mmol, 1 g) and
127 5-Hydroxymethylfurfural (2.4 mmol, 0.30 g) were dissolved in 40 mL absolute
128 ethanol. The mixture was stirred and refluxed for 20 h at 80°C under N_2 atmosphere.
129 Then the solvent was removed under reduced pressure, after cooling to room
130 temperature, and then brown solid was washed with cold ethanol for three times. The
131 crude product recrystallized from 10 mL absolute ethanol, obtaining 0.89 g of RBF
132 (yield 68.5%). IR (KBr) ν_{OH}: 3371cm^{-1}; Mass spectrometry: m/z, calcd: 564.27, found:
133 565.3 ($[M+H]^+$), 587.4 ($[M+Na]^+$). ^1H NMR (400 MHz, $CDCl_3$) δ （ppm）: 8.00-7.98
134 (m, 1H), 7.97 (d, *J* =1.8 Hz, 1H), 7.45 (s, 2H), 7.06 (d, *J* =7.1 Hz, 1H), 6.55 (d, *J* =8.7

Hz, 2H), 6.51 (d, *J* =3.4 Hz, 1H), 6.43 (s, 2H), 6.26 (s, 1H), 6.24 (d, *J* =3.4 Hz, 2H), 4.56 (d, *J* =5.2 Hz, 2H), 3.33 (q, *J* =7.1 Hz, 8H), 2.26 (s, 1H), 1.16 (t, *J* =7.1 Hz, 12H). ^{13}C NMR (100 MHz, DMSO-d_6) δ (ppm): 164.50, 158.63, 152.71, 152.54, 148.90, 138.93, 134.26, 129.05, 128.21, 127.89, 123.90, 123.42, 115.96, 109.87, 108.57, 105.56, 97.96, 65.63, 56.03, 44.12, 12.89.

3. Results and discussion

3.1. Colorimetric recognition of Cu^{2+}

The 3D absorption spectra of RBF (20 μM) toward various metal ions was first explored in Tris-HCl (10 mM, pH=7.20) aqueous buffer solution in the presence of 2 equiv. of different metal ions and the results are shown in Fig. 1A. The probe RBF exhibited a very weak absorption band over 500 nm region, which indicated that probe RBF existed as a spirocycle-closed form [26]. When Cu^{2+} and other metal cations were added into the solution, only the mixture solution with Cu^{2+} exhibited a significant absorbance at 565 nm coupled with an obvious color change from colorless to pink (Fig. 2), which results from the Cu^{2+}-induced ring opening of the spirolactam form. The results showed that probe RBF could be served as a “naked eye” probe with a characteristic of high selectivity toward Cu^{2+} over other competitive metal ions.

3.2. Fluorescence spectral responses of RBF

Changes of fluorescence emission spectra of RBF (10 μM) caused by H^+ (pH=4.50) and various metal ions (20 μM) in B-R buffer solution (pH=7.20) were record in Fig. 1B. The spectrum of RBF showed nearly no fluorescence above 550 nm,

while the addition of H^+ (pH=4.50) caused a strong fluorescence at 591 nm. The fluorescence emission spectra of probe RBF at different pH are shown in Fig. 3A. RBF (10 μM) emitted a very weak fluorescence when the pH value of system was above 6.50, which was ascribed to its spirolactam form in solution. When the value of pH fell to less than 6.50, the fluorescence intensity of probe RBF gradually increased (about 41-fold within the pH range of 7.50-3.73) and the pink color gradually deepen (Fig. 3B), indicating the formation of the ring-opened amide form and highly sensitive to acidic pH.

3.3. The investigation of pH and response time

For practical application, the absorbance intensity response of RBF in the absence and presence of Cu^{2+} in different pH values were evaluated. Increased absorbance intensity of RBF was observed at acidic condition, which was likely due to the H^+-induced ring opening of rhodamine spirolactam. The absorbance intensity of RBF remained stable in a comparatively wide pH range from 7.00 to 10.00 (Fig. 4). However, the addition of Cu^{2+} led to the absorbance enhancement, which was attributed to a Cu^{2+}-induced opening of the rhodamine ring. Therefore, probe RBF was favorable for its application in real samples which exist in neutral conditions.

Fig. 5 shows that the time dependence of the response of RBF (20 μM) to Cu^{2+} (40 μM) was investigated. The absorbance intensity of RBF with Cu^{2+} reached its maximum value at about 30 min, after that the absorbance intensity remained almost constant. Therefore, a 30 min reaction time was selected in subsequent experiments in order to make the metal ions chelated with the sensor sufficiently. Furthermore, we

examined the time course of fluorescence intensity of RBF (10 μM) with pH=4.50 at room temperature. After 2 min, the fluorescence remarkably increased to its maximum value and then remained stable.

3.4. Linearity

To further investigate the interaction of Cu^{2+} with RBF, an absorbance titration experiment was carried out in Tris-HCl (10 mM, pH=7.2) aqueous buffer solution, as shown in Fig. 6, a linear increase of absorbance intensity could be observed under the optimum conditions with increasing Cu^{2+} concentration over a range (0-5 μM), then obtained a detection limit of 0.15 μM based on $3\times\delta_{blank}/k$ (where δ_{blank} is the standard deviation of the blank solution and k is the slope of the calibration plot). The regression equation is Y=0.01816+0.05538X (R=0.9953). Subsequently, as shown in Fig.7, the fluorescence pH titration of RBF exhibited that the fluorescence intensity of RBF were gradually increased about 41-fold within the pH range from 7.50 to 3.73 with a pKa value of 5.02 and linearly proportional (R=0.9924) to pH values in the range from 4.40 to 5.30. The relative fluorescence quantum yields in acidic condition (pH=4.50) were determined to be 0.30 with Rhodamine B (Φ_F=0.97) in ethanol as a standard and calculated using the following equation [62].

$$\Phi_x = \Phi_s \left(\frac{F_x}{F_s}\right)\left(\frac{A_s}{A_x}\right)\left(\frac{\lambda_{exs}}{\lambda_{exx}}\right)\left(\frac{n_x}{n_s}\right)^2$$

Where subscripts X and S refer to the unknown and the standard, Φ stands for quantum yield, F represents integrated area under the emission curve, A is the absorbance intensity at the excitation wavelength, λ_{ex} exhibits the excitation wavelength, n is index of refraction of the solution.

200 3.5. Proposed binding mode

201 As shown in Fig. 8, a Job's plot experiment was established. Total concentration
202 of Cu^{2+} and RBF was maintained constant at 20 μM and mole fraction of Cu^{2+}
203 changed from 0 to 1. The maximum absorbance intensity at 565 nm was appeared
204 when the molecular fraction of Cu^{2+} was close to 0.33, which indicated that the 1:2
205 stoichiometry was the most possible binding mode of Cu^{2+} and RBF.

206 In order to better understand the complexation behavior of Cu^{2+} with RBF, the
207 ESI-MS experiment was conducted to prove the reaction mechanism [42]. As shown
208 in Fig. 9, the peak at m/z=565.3 and 587.4 corresponded to $[RBF+H]^+$ and $[RBF+Na]^+$,
209 respectively. And the peak at m/z=596.3 corresponded to $[2(RBF-H)+Cu+2H]^{2+}$. The
210 results supported the 1:2 stoichiometry of the Cu^{2+} to RBF complex concluded from
211 the Job's plot.

212 3.6. Reversibility and reaction mechanism

213 As shown in Fig. 10, the EDTA-adding experiment was implemented to analyze
214 the chemical stability and reversibility behavior of the binding of RBF and Cu^{2+}. The
215 absorbance intensity of the mixture solution of RBF and Cu^{2+} was significant
216 decreased when excess EDTA was added, then signals were almost completely
217 restored when excess Cu^{2+} was added to the system. The results also further indicated
218 that the spectral response of RBF to Cu^{2+} was likely due to the chelation-induced ring
219 opening of rhodamine spirolactam, rather than other possible reactions [46].
220 Furthermore, Fig. 11 shows that the fluorescence intensity of the chemosensor was
221 reversible between pH 4.50 and 7.20, which means it was suitable for the detection of

a system with a shifty pH value. As the above (Figs. 8, 9, 10 and 11), the possible coordination modes of RBF for H^+ and Cu^{2+} were proposed in the Scheme 2.

3.7. Tolerance of RBF to Cu^{2+} and pH over other metal ions

The effects of other metal ions on Cu^{2+} and pH measurements were evaluated through competitive experiments. As shown in Fig. 12, the absorbance intensity changes of RBF (20 μM) in Tris-HCl (10 mM, pH=7.20) aqueous buffer solution were measured by the treatment of Cu^{2+} (40 μM) in the presence of other interfering metal ions (40 μM) including Pb^{2+}, Na^+, K^+, Cd^{2+}, Ba^{2+}, Zn^{2+}, Mg^{2+}, Ag^+, Ni^{2+}, Ca^{2+}, Al^{3+}, Cr^{3+} and Fe^{3+}. The results indicated that the recognition of Cu^{2+} by RBF was hardly affected by other coexisting metal ions. Moreover, Fig. 13 shows that the fluorescent selectivity of RBF for H^+ at different pH values. Except Cu^{2+} caused fluorescence quenching to different degrees, the addition of Pb^{2+}, Na^+, K^+, Cd^{2+}, Ba^{2+}, Zn^{2+}, Mg^{2+}, Ag^+, Ni^{2+}, Ca^{2+}, Al^{3+}, Cr^{3+} and Fe^{3+} had no effect on fluorescence intensity in B-R buffer solution at pH 7.20 and 4.50. Because of the low content of Cu^{2+} within cells, this quenching did not affect cell imaging [50].

3.8. Laser scanning confocal microscopy experiments of PC12 and Hela cells

We used RBF with PC12 cells (A) and Hela cells (B) to investigate the potential biological application of RBF for fluorescence imaging. PC12 cells and Hela cells were incubated with RBF (10 μM) at different incubation time (0.5, 1, 1.5 h) at 37°C, respectively. As shown in Fig. 14, after three times washed with Tris-HCl buffer solutions, the blank 1 and blank 2 groups without RBF exhibited no fluorescence, and other groups showed the increase of fluorescence intensity with increasing time (Fig.

14a, b, c and a_i, b_i, c_i). The different fluorescence intensity within individual cell demonstrated that intracellular pH is not equably distributed [50]. Bright-field measurements after treatment with RBF confirmed that the PC12 cells and Hela cells were viable throughout the imaging experiments (Fig. 14d, e, f and d_i, e_i, f_i). The above facts indicated that probe RBF showed excellent cell membrane permeability and staining ability in living cells.

3.9. Preliminary analytical application

In order to investigate the applicability of the proposed method in real sample analysis, the chemosensor RBF was applied in the determination of Cu^{2+} in lake water which collected from the campus of Henan university and tap water samples. Then the lake water was simply filtered. All these samples were adjusted pH by Tris-HCl (10 mM, pH=7.2) aqueous buffer solution. As shown in Table 1, Cu^{2+} was undetected from both of the lake water and tap water. Moreover, the results showed satisfactory recovery and R.S.D. values for all of the samples. As a consequence, RBF seems available to detect Cu^{2+} in lake water and tap water.

4. Conclusion

In summary, we have designed and synthesized a dual-function rhodamine B-based fluorescent chemosensor (RBF). RBF exhibited specific fluorescent response to acidic pH and reversibility between pH 4.50 and 7.20. The fluorescence intensity of RBF exhibited a more than 41-fold increase within the pH range from 7.50 to 3.73 with a pKa value of 5.02, and also showed a clear color change from colorless to pink, which was very available to monitor intracellular pH in living PC12 cells and Hela

cells. Moreover, RBF showed highly sensitive and selective colorimetric recognition of Cu^{2+}, which could be served as a “naked eye” probe. It has been successfully applied to detect Cu^{2+} in real water samples.

Acknowledgement

The authors are grateful for the base and cutting-edge technology research project of Henan province (142300410369), the natural science research project of Henan province education department (2014A610013).

References

[1] J.M. Zen, G. Patonay, Anal. Chem. 63 (1991) 2934-2938.

[2] E. Hillborn, J. Lldén, S. Pettersson, Anal. Chem. 55 (1983) 1180-1182.

[3] G. Ke, Z. Zhu, W. Wang, Y. Zou, Z. Guan, S. Jia, H. Zhang, X. Wu, C.J. Yang, ACS Appl. Mater. Inter. 6 (2014) 15329-15334.

[4] W.M. Liu, P.H. Keizers, M.A. Hass, A. Blok, M. Timmer, A.J.C. Sarris, M. Overhand, M. Ubbink, J. Am. Chem. Soc. 134 (2012) 17306-17313.

[5] A. Roos, W.F. Boron, Physiol. Rev. 61 (1981) 296-434.

[6] F. Han, Y. Xu, D. Jiang, Y. Qin, H. Chen, Anal. Biochem. 435 (2013) 106-113.

[7] D. Perezsala, D. Colladoescobar, F. Mollinedo, J. Biol. Chem. 270 (1995) 6235-6242.

[8] S. Humez, M. Monet, F. van Coppenolle, P. Delcourt, N. Prevarskaya, Am. J. Physiol. Cell Physiol. 287 (2004) C1733-C1746.

[9] R. Martínez-Zaguilán, B.F. Chinnock, S. Wald-Hopkins, M. Bernas, D. Way, M. Weinand, M.H. Witte, R.J. Gillies, Cell. Physiol. Biochem. 6 (1996) 169-184.

[10] S.H. Yoo, Y.S. Hur, Cell Calcium 51 (2012) 342-350.

[11] A.P. Lieberman, R. Puertollano, N. Raben, S. Slaugenhaupt, S.U. Walkley, A. Ballabio, Autophagy 8 (2014) 719-730.

[12] J. Suk, S.S. Kwak, J.H. Lee, J.H. Choi, S.H. Lee, D.H. Lee, B. Byun, G.H. Lee, C.O. Joe, J. Cell Biochem. 112 (2011) 2566-2573.

[13] R.J. GILLIES, K. UGURBIL, J.A. DEN HOLLANDER, R.G. SHULMAN, Proc. Natl. Acad. Sci.USA 78 (1981) 2125-2129.

[14] D. ELLIS, R.C. THOMAS, Nature 262 (1976) 224-225.

[15] P. Gameiro, S. Reis, J.L.F.C. Lima, B. Castro, Anal. Chim. Acta 405 (2000) 167-172.

[16] N. Balazs, P. Sipos, Carbohydr. Res. 342 (2007) 124-130.

[17] E. Gaggelli, H. Kozlowski, D. Valensin, G. Valensin, Chem. Rev. 106 (2006) 1995-2044.

[18] J. Wang, L. Long, D. Xie, X. Song, Sens. Actuators B: Chem. 177 (2013) 27-33.

[19] I. Paris, J. Segura-Aguilar, Monatsh. Chem. 142 (2011) 365-374.

[20] K.J. Barnham, C.L. Masters, A.I. Bush, Nat. Rev. Drug Discov. 3 (2004) 205-214.

[21] W.I.M. Vonk, P. de Bie, C.G.K. Wichers, P.V.E. van den Berghe, R. van der Plaats, R. Berger, C. Wijmenga, L.W.J. Klomp, B. van de Sluis, Cell. Mol. Life S. 69 (2012) 149-163.

[22] Y.J. Kang, Pharmacol. Therapeut. 129 (2011) 321-331.

[23] P. Puangploy, S. Smanmoo, W. Surareungchai, Sens. Actuators B: Chem. 193 (2014) 679-686.

[24] J. Liu, G. Liu, W. Liu, Y. Wang, Biosens. Bioelectron. 64C (2014) 300-305.

[25] W.Y. Liu, S.L. Shen, H.Y. Li, J.Y. Miao, B.X. Zhao, Anal. Chim. Acta 791 (2013) 65-71.

[26] K. Bera, A.K. Das, M. Nag, S. Basak, Anal. Chem. 86 (2014) 2740-2746.

[27] S.K. Ko, Y.K. Yang, J. Tae, I. Shin, J. Am. Chem. Soc. 128 (2006) 14150-14155.

[28] Y.K. Yang, K.J. Yook, J. Tae, J. Am. Chem. Soc. 127 (2005) 16760-16761.

[29] M. Kumar, N. Kumar, V. Bhalla, H. Singh, P.R. Sharma, T. Kaur, Org. Lett. 13 (2011) 1422-1425.

[30] M. Wang, F.-Y. Yan, Y. Zou, N. Yang, L. Chen, L.-G. Chen, Spectrochim. Acta A: Mol. Biomol. Spectrosc. 123 (2014) 216-223.

[31] S.B. Maity, P.K. Bharadwaj, Inorg. Chem. 52 (2013) 1161-1163.

[32] A. Sahana, A. Banerjee, S. Lohar, B. Sarkar, S.K. Mukhopadhyay, D. Das, Inorg. Chem. 52 (2013) 3627-3633.

[33] A. Dhara, A. Jana, S. Konar, S.K. Ghatak, S. Ray, K. Das, A. Bandyopadhyay, N. Guchhait, S.K. Kar, Tetrahedron Lett. 54 (2013) 3630-3634.

[34] Z. Li, Q. Hu, C. Li, J. Dou, J. Cao, W. Chen, Q. Zhu, Tetrahedron Lett. 55 (2014) 1258-1262.

[35] F. Ge, H. Ye, H. Zhang, B.X. Zhao, Dyes Pigm. 99 (2013) 661-665.

[36] Y.X. Wu, J.B. Li, L.H. Liang, D.Q. Lu, J. Zhang, G.J. Mao, L.Y. Zhou, X.B. Zhang, W. Tan, G.L. Shen, R.Q. Yu, Chem. Commun. 50 (2014) 2040-2042.

[37] C.Y. Li, C.X. Zou, Y.F. Li, J.L. Tang, C. Weng, Dyes Pigm. 104 (2014) 110-115.

[38] L.-Q. Li, L.-P. Meng, Spectrochim. Acta A: Mol. Biomol. Spectrosc. 122 (2014) 772-775.

[39] Y. Wan, Q. Guo, X. Wang, A. Xia, Anal. Chim. Acta 665 (2010) 215-220.

[40] Y. Zhou, J. Zhang, L. Zhang, Q. Zhang, T. Ma, J. Niu, Dyes Pigm. 97 (2013) 148-154.

[41] V. Dujols, F. Ford, A.W. Czarnik, J. Am. Chem. Soc. 119 (1997) 7386-7387.

[42] J. Yin, X. Ma, G. Wei, D. Wei, Y. Du, Sens. Actuators B: Chem. 177 (2013)

213-217.

[43] M. Kumar, N. Kumar, V. Bhalla, P.R. Sharma, T. Kaur, Org. Lett. 14 (2012) 406-409.

[44] Z. Jiang, S. Tian, C. Wei, T. Ni, Y. Li, L. Dai, D. Zhang, Sens. Actuators B: Chem. 184 (2013) 106-112.

[45] J. Xu, Y. Hou, Q. Ma, X. Wu, S. Feng, J. Zhang, Y. Shen, Spectrochim. Acta A: Mol. Biomol. Spectrosc. 124 (2014) 416-422.

[46] L. Tang, X. Dai, X. Wen, D. Wu, Q. Zhang, Spectrochim. Acta A: Mol. Biomol. Spectrosc.139 (2015) 329-334.

[47] S. Cai, Y. Lu, S. He, F. Wei, L. Zhao, X. Zeng, Chem. Commun. 49 (2013) 822-824.

[48] A. Liu, M. Hong, W. Yang, S. Lu, D. Xu, Tetrahedron 70 (2014) 6974-6979.

[49] J.-L. Tan, M.-X. Zhang, F. Zhang, T.-T. Yang, Y. Liu, Z.-B. Li, H. Zuo, Spectrochim. Acta A: Mol. Biomol. Spectrosc. 140 (2015) 489-494.

[50] H.S. Lv, S.Y. Huang, B.X. Zhao, J.Y. Miao, Anal. Chim. Acta 788 (2013) 177-182.

[51] J.-L. Tan, M.-X. Zhang, F. Zhang, T.-T. Yang, Y. Liu, Z.-B. Li, H. Zuo, Spectrochim. Acta A: Mol. Biomol. Spectrosc. 140 (2015) 489-494.

[52] Z.Q. Hu, M. Li, M.D. Liu, W.M. Zhuang, G.K. Li, Dyes Pigm. 96 (2013) 71-75.

[53] H.S. Lv, J. Liu, J. Zhao, B.X. Zhao, J.Y. Miao, Sens. Actuators B: Chem. 177 (2013) 956-963.

[54] H.S. Lv, S.Y. Huang, Y. Xu, X. Dai, J.Y. Miao, B.X. Zhao, Bioorg. Med. Chem.

Lett. 24 (2014) 535-538.

[55] Y. Lv, L. Zhu, H. Liu, Y. Wu, Z. Chen, H. Fu, Z. Tian, Anal. Chim. Acta 839 (2014) 74-82.

[56] N.R. Chereddy, K. Saranraj, A.K. Barui, C.R. Patra, V.J. Rao, S. Thennarasu, RSC Adv. 4 (2014) 24324.

[57] P. Mahato, S. Saha, E. Suresh, R. Di Liddo, P.P. Parnigotto, M.T. Conconi, M.K. Kesharwani, B. Ganguly, A. Das, Inorg. Chem. 51 (2012) 1769-1777.

[58] M. Wang, F. Yan, Y. Zou, L. Chen, N. Yang, X. Zhou, Sens. Actuators B: Chem. 192 (2014) 512-521.

[59] S. Saha, P. Mahato, G.U. Reddy, E. Suresh, A. Chakrabarty, M. Baidya, S.K. Ghosh, A. Das, Inorg. Chem. 51 (2012) 336-345.

[60] C.C. Ju, H.J. Yin, C.L. Yuan, K.Z. Wang, Spectrochim. Acta A: Mol. Biomol. Spectrosc.79 (2011) 1876-1880.

[61] Y. Xiang, L. Mei, N. Li, A.J. Tong, Anal. Chim. Acta 581 (2007) 132-136.

[62] S. Sun, B. Qiao, N. Jiang, J. Wang, S. Zhang, X. Peng, Org. Lett. 16 (2014) 1132-1135.

Figure captions:

Scheme 1. Synthesis of RBF

Fig. 1. (A) UV-Vis absorbance spectra of RBF (20 μM) in Tris-HCl buffer solution (10 mM, pH=7.20) upon addition of different metal ions (40 μM). (B) Fluorescence spectra of RBF (10 μM) with the presence of H^+ in B-R buffer solution (pH=4.50) and various metal ions (20 μM) in B-R buffer solution (pH=7.20).

Fig. 2. Colors of RBF (20 μM) and RBF with different metal ions (40 μM).

Fig. 3. (A) Fluorescent spectra of RBF (10 μM) in B-R buffer with different pH, λ_{ex}=520 nm. (B) (a) Changes of color of RBF (10 μM) in B-R buffer with different pH. (b) Changes of Fluorescent intensity of RBF (10 μM) in B-R buffer with different pH.

Fig. 4. Absorption intensity (565 nm) of free RBF (20 μM) and RBF+2 equiv. Cu^{2+} in Tris-HCl buffer solution with different pH conditions.

Fig. 5. (a): The time courses of fluorescence intensity of RBF (10 μM) in B-R buffer solution (pH=4.50); (b): The time courses of absorbance intensity of RBF (20 μM) in Tris-HCl buffer solution (10 mM, pH=7.20).

Fig. 6. Absorbance spectra of reaction solution of RBF (20 μM) in Tris-HCl buffer solution (10 mM, pH=7.20) with different concentrations of Cu^{2+}. Inset: absorbance at 565 nm as a function of Cu^{2+} concentration.

Fig. 7. Fluorescence intensity at 591 nm (λ_{ex}=520 nm) by pH values according to the fluorescent pH titration (pH 3.73-7.50). The inset shows the linear relationship of fluorescence intensity at 591 nm and pH values from 4.40 to 5.30.

Fig. 8. Job's plot of the complex formed by $[Cu^{2+}]/[Cu^{2+}]+[RBF]$. The total

concentration of RBF and Cu^{2+} was 20 μM.

Fig. 9. ESI-MS spectrum of reaction between RBF and Cu^{2+}: (A) RBF (40 μM), (B) RBF with 2 equiv. of Cu^{2+}.

Fig. 10. Absorbance spectra showing reversibility of Cu^{2+} coordination to RBF by EDTA in Tris-HCl (10 mM, pH=7.20) buffer solution. (a): only RBF (20 μM); (b): RBF+2 equiv. Cu^{2+}; (c): RBF+2 equiv. Cu^{2+}+5 equiv. EDTA; (d): RBF+2 equiv. Cu^{2+}+5 equiv. EDTA+7 equiv. Cu^{2+}; (e): RBF+2 equiv. Cu^{2+}+5 equiv. EDTA+9 equiv. Cu^{2+};

Fig. 11. pH reversibility study of RBF (10 μM) between pH 7.20 and 4.50.

Scheme 2. Proposed mechanism of RBF for H^{+} and Cu^{2+} respectively.

Fig. 12. Metal ions selectivity of RBF (20 μM) in Tris-HCl (10 mM, pH=7.20) buffer solution. The black bars represent the absorbance intensity of the solution containing RBF (20 μM) and different metal ions (40 μM). The red bars represent the absorbance intensity changes that occur upon addition of Cu^{2+} (40 μM) to the solution containing RBF and different metal ions.

Fig. 13. (A) Emission change at 591 nm of **RBF** (10 μM) in the presence of different metal ions in B-R buffer solution at pH 7.20, λ_{ex}=520 nm. (B) Emission change at 591 nm of **RBF** (10 μM) in the presence of different metal ions in B-R buffer solution at pH 4.50, λ_{ex}=520 nm. The final concentration of K^{+}, Na^{+}, Ca^{2+} and Mg^{2+} are 200 μM, respectively, while that of other metal ions are 50 μM.

Fig. 14. Confocal fluorescence images of PC12 cells (A) and Hela cells (B) (λ_{ex}=515 nm). Blank 1 and Blank 2: Only PC12 cells and Hela cells without probe RBF,

442 respectively. (a), (b) and (c) of PC12 cells incubated with probe RBF (10 μM) for 0.5
443 h, 1 h and 1.5 h at 37 ˚C, respectively. (a_i), (b_i) and (c_i) of Hela cells incubated with
444 probe RBF (10 μM) for 0.5 h, 1 h and 1.5 h at 37 ˚C, respectively., (d), (e), (f) and (d_i)
445 (e_i) (f_i): Bright-field view of panel. (g), (h), (i) and (g_i), (h_i) (i_i): Overlay image of dark
446 field and bright field.

Figure(s)

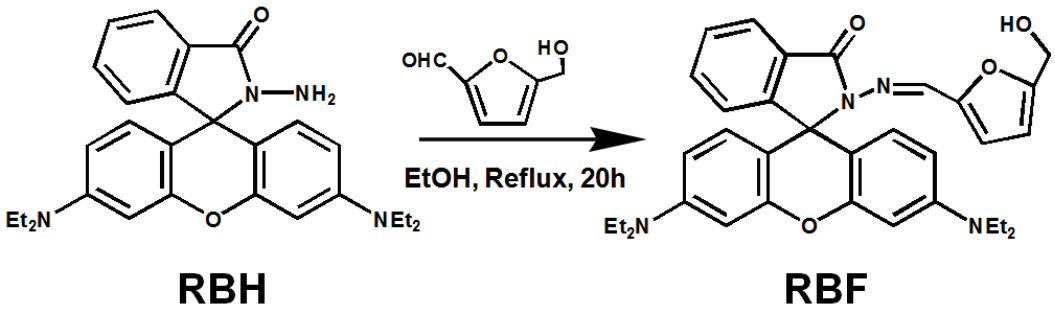

Scheme 1. Synthesis of RBF

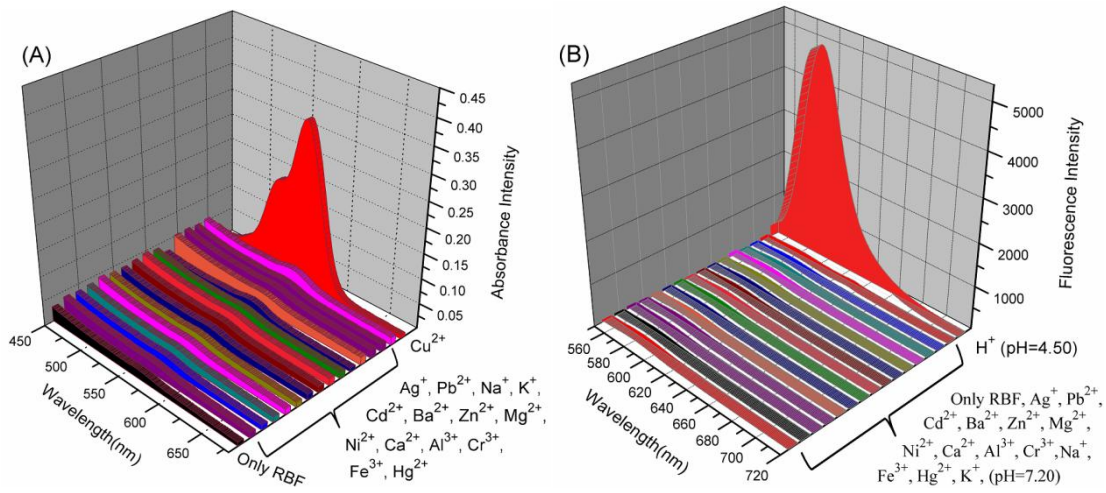

Fig. 1. (A) UV-Vis absorbance spectra of RBF (20 μM) in Tris-HCl buffer solution (10 mM, pH=7.20) upon addition of different metal ions (40 μM). (B) Fluorescence spectra of RBF (10 μM) with the presence of H^+ in B-R buffer solution (pH=4.50) and various metal ions (20 μM) in B-R buffer solution (pH=7.20).

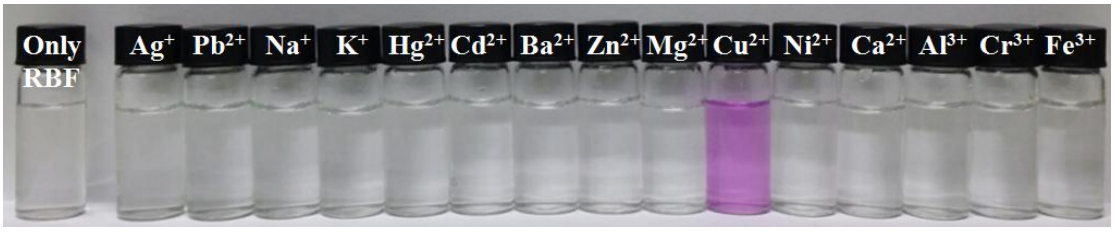

Fig. 2. Colors of RBF (20 μM) and RBF with different metal ions (40 μM).

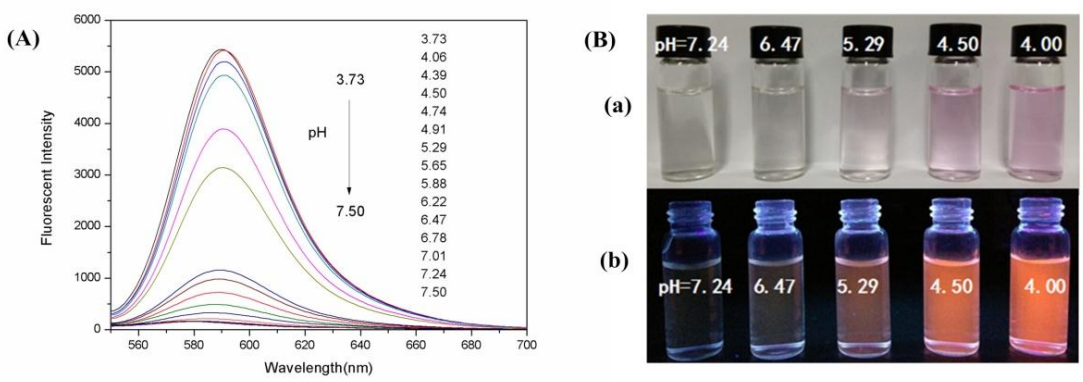

Fig. 3. (A) Fluorescent spectra of RBF (10 μM) in B-R buffer with different pH, λ_{ex}=520 nm. (B) (a) Changes of color of RBF (10 μM) in B-R buffer with different pH. (b) Changes of Fluorescent intensity of RBF (10 μM) in B-R buffer with different pH.

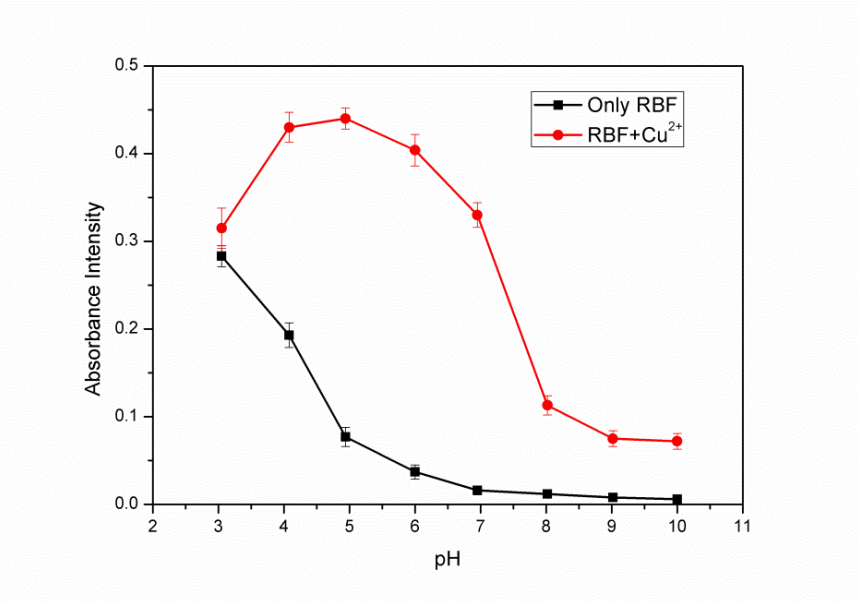

Fig. 4. Absorption intensity (565 nm) of free RBF (20 μM) and RBF+2 equiv. Cu^{2+} in Tris-HCl buffer solution with different pH conditions.

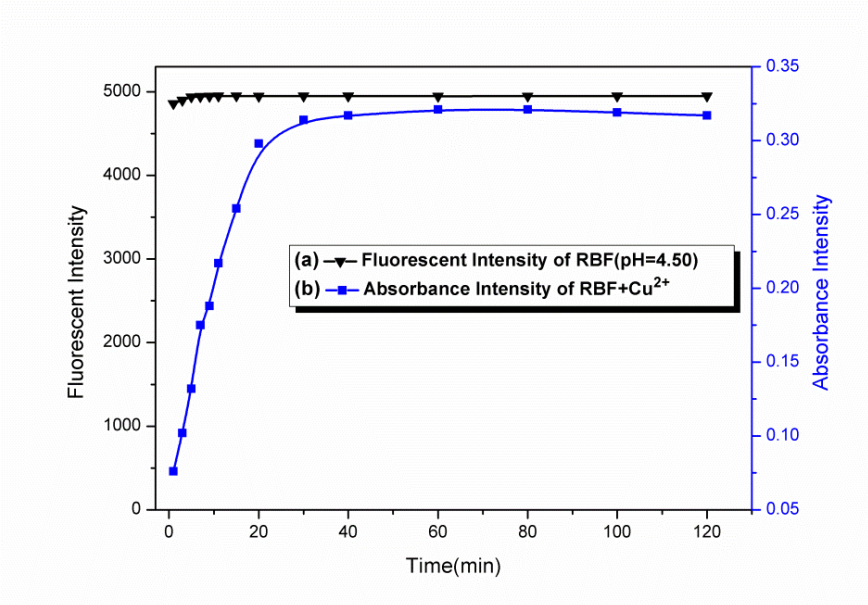

Fig. 5. (a): The time courses of fluorescence intensity of RBF (10 μM) in B-R buffer solution (pH=4.50); (b): The time courses of absorbance intensity of RBF (20 μM) in Tris-HCl buffer solution (10 mM, pH=7.20).

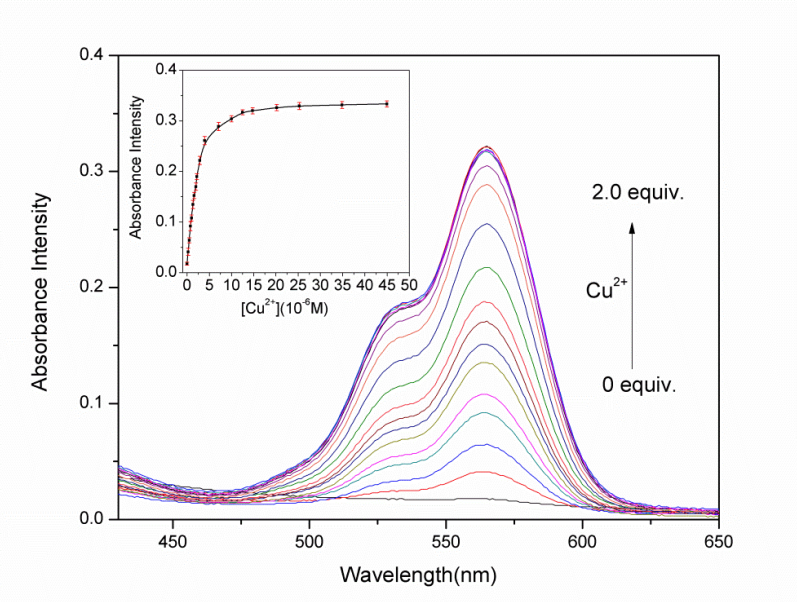

Fig. 6. Absorbance spectra of reaction solution of RBF (20 μM) in Tris-HCl buffer solution (10 mM, pH=7.20) with different concentrations of Cu^{2+}. Inset: absorbance at 565 nm as a function of Cu^{2+} concentration.

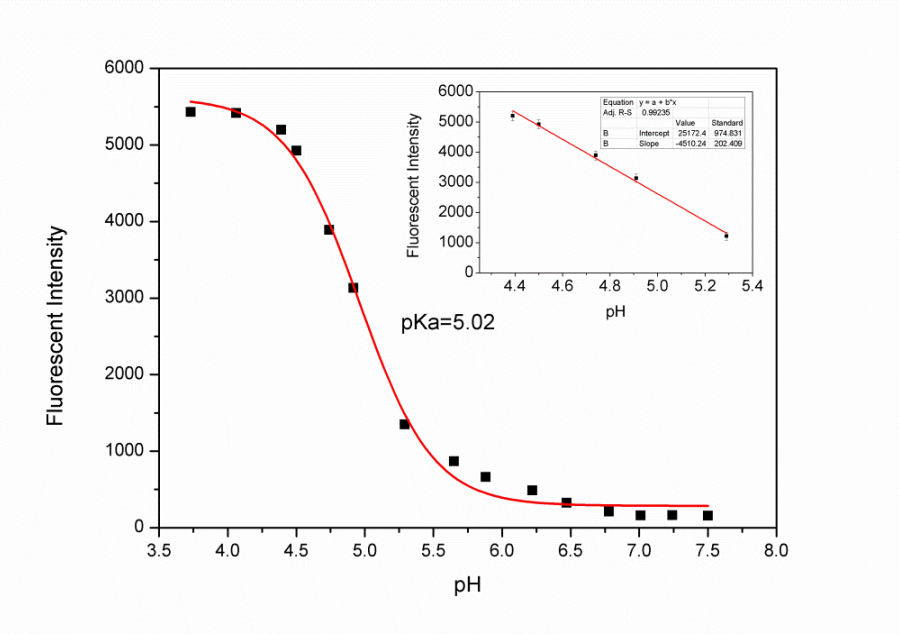

Fig. 7. Fluorescence intensity at 591 nm (λ_{ex}=520 nm) by pH values according to the fluorescent pH titration (pH 3.73-7.50). The inset shows the linear relationship of fluorescence intensity at 591 nm and pH values from 4.40 to 5.30

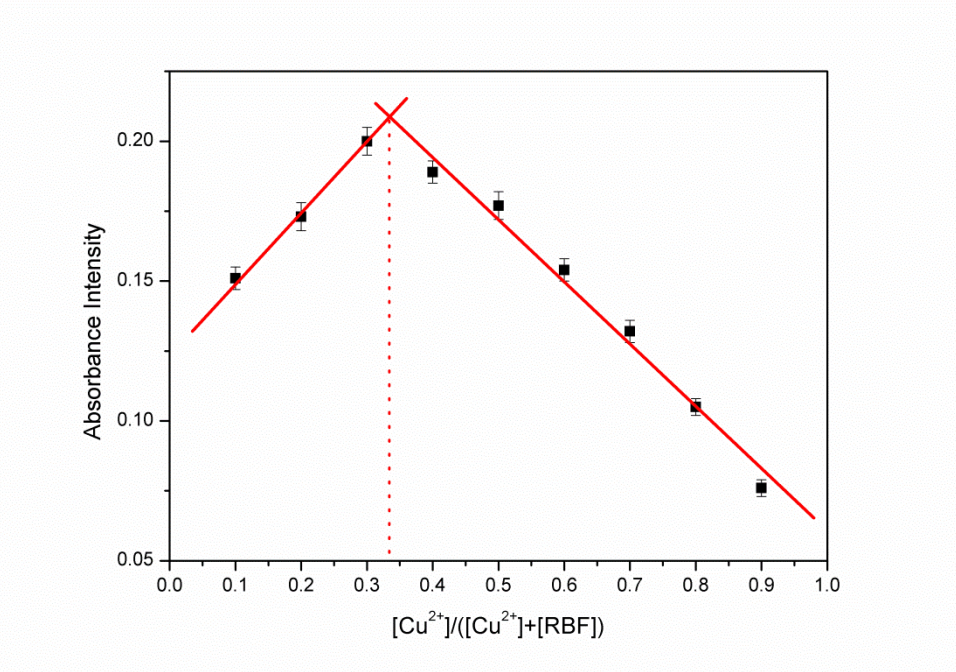

Fig. 8. Job's plot of the complex formed by $[Cu^{2+}]/[Cu^{2+}]+[RBF]$. The total concentration of RBF and Cu^{2+} was 20 μM.

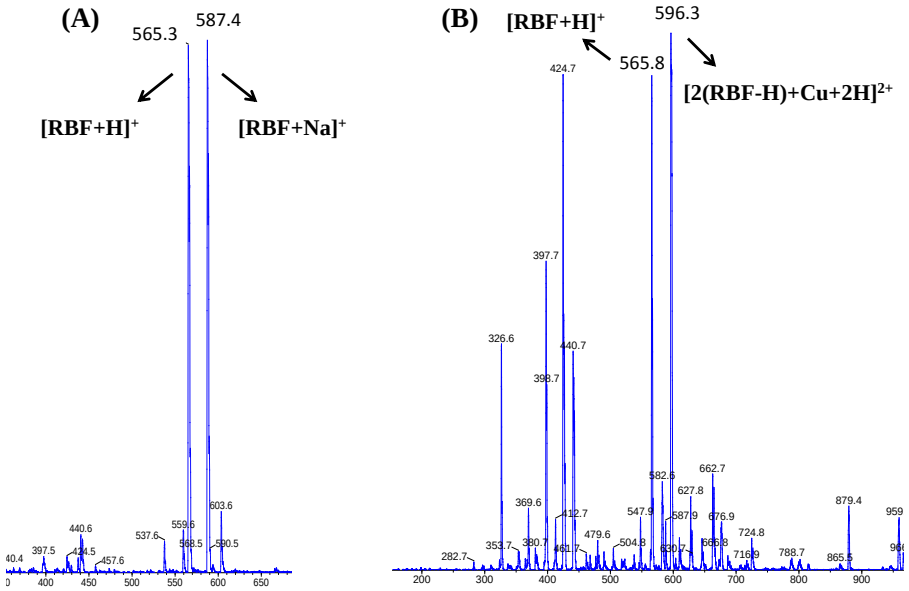

Fig. 9. ESI-MS spectrum of reaction between RBF and Cu^{2+}: (A) RBF (40 μM), (B) RBF with 2 equiv. of Cu^{2+}.

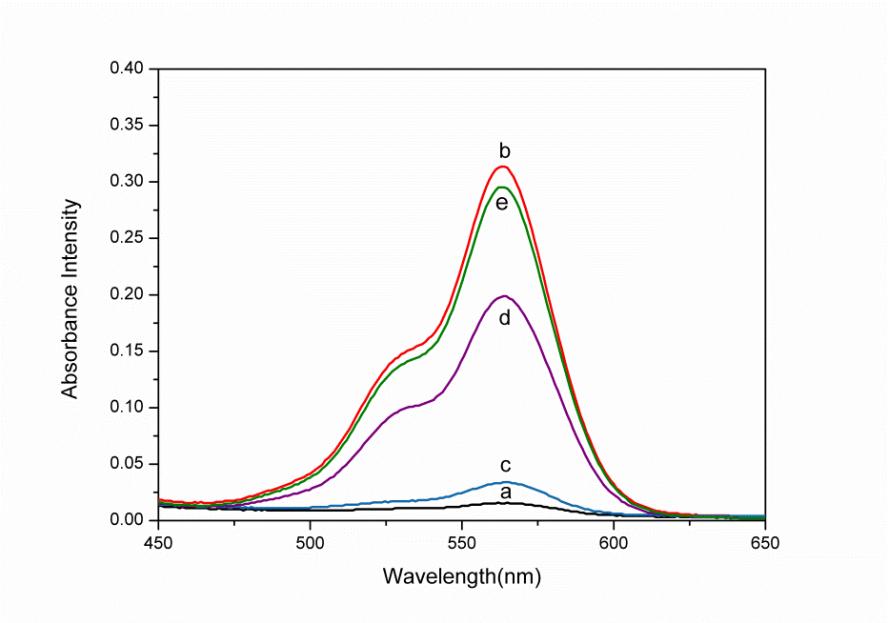

Fig. 10. Absorbance spectra showing reversibility of Cu^{2+} coordination to RBF by EDTA in Tris-HCl (10 mM, pH=7.20) buffer solution. (a): only RBF (20 μM); (b): RBF+ 2 equiv. Cu^{2+}; (c): RBF+2 equiv. Cu^{2+}+5 equiv. EDTA; (d): RBF+2 equiv. Cu^{2+}+5 equiv. EDTA+7 equiv. Cu^{2+}; (e): RBF+2 equiv. Cu^{2+}+5 equiv. EDTA+9 equiv. Cu^{2+};

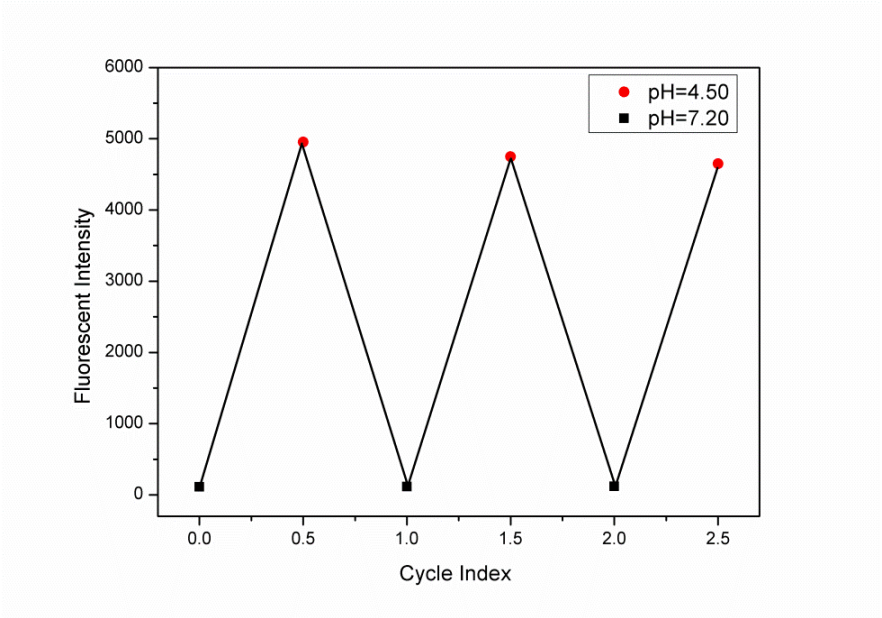

Fig. 11. pH reversibility study of RBF (10 μM) between pH 7.20 and 4.50.

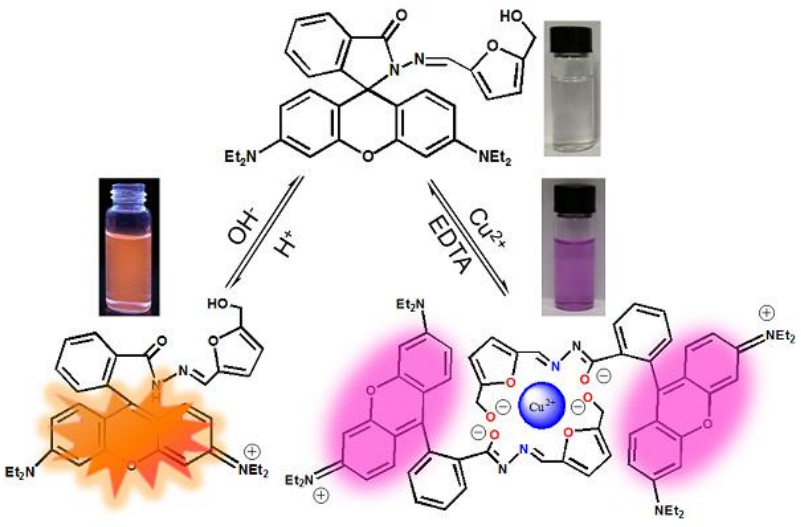

Scheme 2. Proposed mechanism of RBF for H^+ and Cu^{2+} respectively.

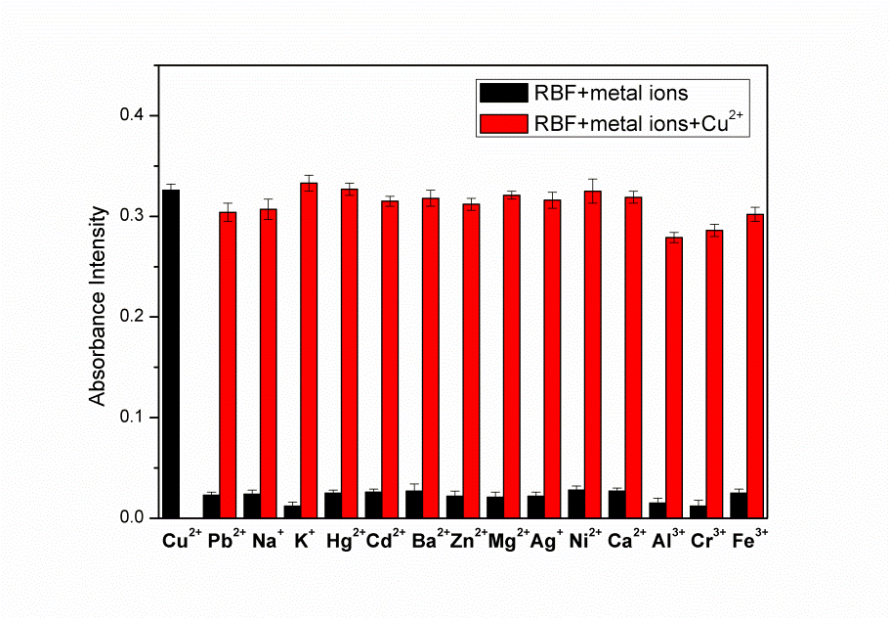

Fig. 12. Metal ions selectivity of RBF (20 μM) in Tris-HCl (10 mM, pH=7.20) buffer solution. The black bars represent the absorbance intensity of the solution containing RBF (20 μM) and different metal ions (40 μM). The red bars represent the absorbance intensity changes that occur upon addition of Cu^{2+} (40 μM) to the solution containing RBF and different metal ions.

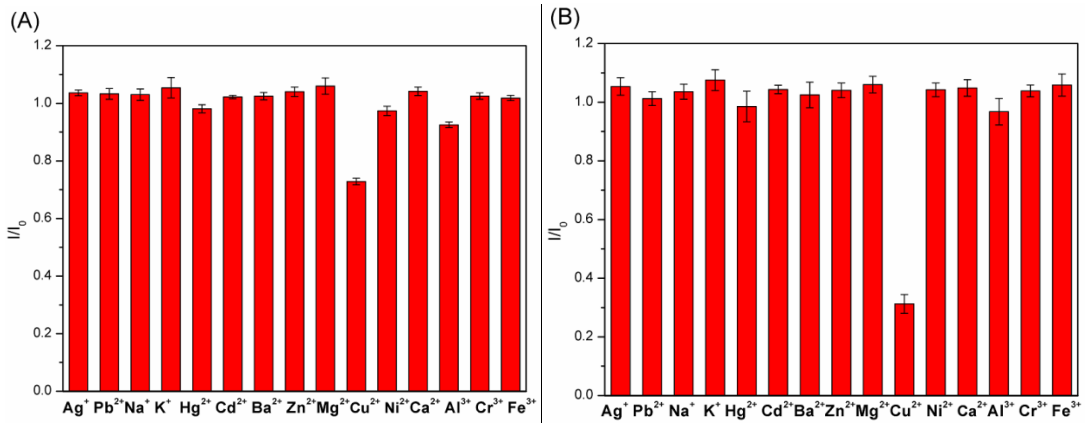

Fig. 13. (A) Emission change at 591 nm of RBF (10 μM) in the presence of different metal ions in B-R buffer solution at pH 7.20, λ_{ex}=520 nm. (B) Emission change at 591 nm of RBF (10 μM) in the presence of different metal ions in B-R buffer solution at pH 4.50, λ_{ex}=520 nm. The final concentration of K^+, Na^+, Ca^{2+} and Mg^{2+} are 200 μM, respectively, while that of other metal ions are 50 μM.

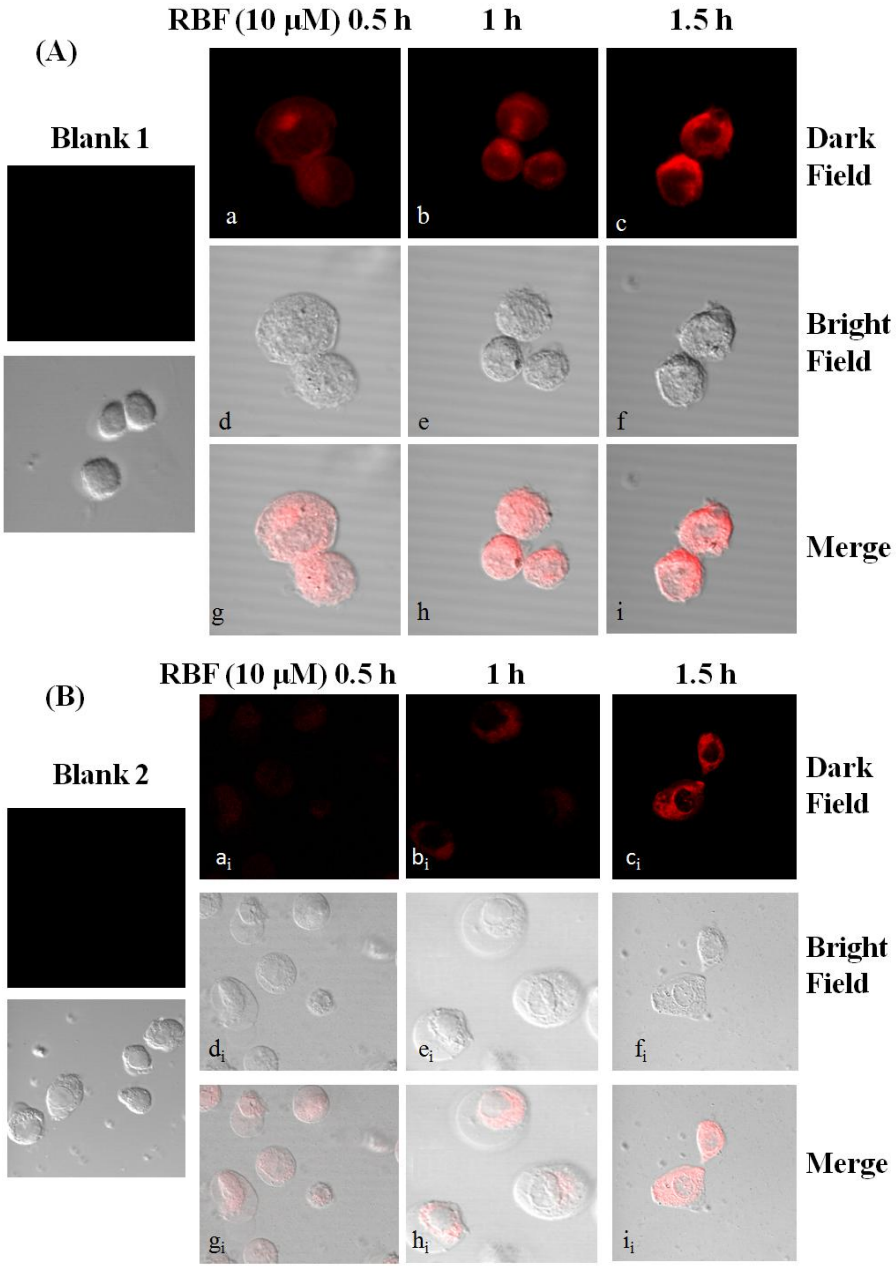

Fig. 14. Confocal fluorescence images of PC12 cells (A) and Hela cells (B) (λ_{ex}=515 nm). Blank 1 and Blank 2: Only PC12 cells and Hela cells without probe RBF, respectively. (a), (b) and (c) of PC12 cells incubated with probe RBF (10 μM) for 0.5 h, 1 h and 1.5 h at 37 °C, respectively. (a_i), (b_i) and (c_i) of Hela cells incubated with probe RBF (10 μM) for 0.5 h, 1 h and 1.5 h at 37 °C, respectively., (d), (e), (f) and (d_i) (e_i) (f_i): Bright-field view of panel. (g), (h), (i) and (g_i), (h_i) (i_i): Overlay image of dark field and bright field.

Table(s)

Table 1. Determination of Cu^{2+} in samples (n = 5).

Sample	Cu^{2+} added (μM)	Cu^{2+} found (μM)	Recovery (%)	R.S.D. (%)
Lake water	0	Undetected	-	-
	0.25	0.253	101.2	2.3
	1.25	1.220	97.6	1.8
Tap water	0	Undetected	-	-
	0.25	0.241	96.2	2.8
	1.25	1.231	98.5	2.6